Jinst

Published by IOP Publishing for Sissa Medialab

Received: *September 27, 2019*
Revised: *November 25, 2019*
Accepted: *January 14, 2020*
Published: *March 2, 2020*

21st International Workshop on Radiation Imaging Detectors
7–12 July 2019
Crete, Greece

Super-resolution X-ray imaging with hybrid pixel detectors using electromagnetic source stepping

T. Dreier,[a,b,1] **U. Lundström**[b] **and M. Bech**[a]

[a] *Lund University, Clinical Sciences Lund, Department for Medical Radiation Physics, Barngatan 4, 222 42 Lund, Sweden*
[b] *Excillum AB, Jan Stenbecks Torg 17, 164 40 Kista, Sweden*

E-mail: till.dreier@med.lu.se

Abstract: With increasing demand for high-resolution X-ray images, the super-resolution method allows to estimate a single high-resolution image from several low-resolution images. Hybrid pixel detectors provide high-quality and low-resolution images, which makes them particularly well suited for super-resolution. However, such detectors consist of a limited number of pixels at high cost.

Applying super-resolution with hybrid pixel detectors shows that it is a viable method to obtain high-resolution images. The point-spread function of such detectors can be idealised to be 1 pixel, adding no blur into the image making such detectors the ideal choice for the application of super-resolution X-ray imaging. However, there are charge sharing effects between the pixels caused by the energy and impact position of incoming photons.

Utilising an X-ray source, which allows magnetic stepping of the X-ray spot, several slightly shifted images can be obtained without requiring mechanical movements. Registering the shifts between individual images with sub-pixel precision allows to estimate a high-resolution image. With repeatable and equally spaced X-ray spot position patterns, sufficient information can be obtained with only a few images. In this paper, we present the application of super-resolution for X-ray imaging using a Pilatus 100K hybrid pixel detector from Dectris Ltd. and a prototype micro-focus X-ray source from Excillum AB. Moreover, we analyse the image quality for applications in X-ray radiography and tomography.

Using a sufficient number of low-resolution images allows us to achieve an increase in resolution, without introducing significant blur or artefacts into the image. Here we quantify the effects on the quality of resulting super-resolution images using different methods of image interpolation, interpolation factors, shifts of the sample on the detector, and amount of low-resolution images.

Keywords: Computerized Tomography (CT) and Computed Radiography (CR); Data processing methods; X-ray detectors; X-ray generators and sources

[1] Corresponding author.

https://doi.org/10.1088/1748-0221/15/03/C03002

Contents

2020 JINST 15 C03002

1 Introduction

For most imaging applications, resolution and contrast are the most significant aspects. Thus, their enhancement is subject to continuous optimisation and development. Super-resolution describes a method estimating one high-resolution image using several slightly shifted low resolution images [1]. This method provides an approach to increase the resolution using a series of images. However, for biological samples, which suffer from radiation damage, efficiency needs to be considered as well.

Using a micro-focus solid anode source prototype from Excillum with a spot size of 10 μm *full width at half maximum* (FWHM) and an acceleration voltage of 70 kV. Using the source's advanced electron optics allows to precisely deflect the electron beam resulting in a movable X-ray spot [2]. Utilising a grid pattern of X-ray spot positions assures that sufficient new information are contained in each individual image.

The use of hybrid pixel detectors is specifically beneficial for the application of super-resolution imaging. Typically, super-resolution imaging requires post-processing of the estimated high-resolution image using a deconvolution filter [1] to reduce blurring by the *point spread function* (PSF) of the detector. Contrary to CMOS or CCD cameras, pixel detectors have a PSF of a single pixel, i.e. the resulting image is not blurred by the detector's PSF.

The source spot rescaled to the detector plane has to be smaller than the pixel size to avoid blurring from the X-ray source. In this case, post-processing of the high-resolution image can be neglected since no additional blur has been induced by the detector nor the source.

2 Methods

2.1 Imaging setup

The lab setup consists of an Excillum micro-focus prototype source with a solid anode. The source allows precise electromagnetic stepping of the X-ray spot, which can be focused to 10 µm FWHM at an acceleration voltage of 70 kV. As detector, a Pilatus 100K from Dectris Ltd. is used. The detector consists of 487 × 195 pixels with a pitch of 172 µm and a 1 mm thick Silicon sensor [3]. Further, the detector is placed 1.5 m away from the source [2].

In this paper, 2 different samples are used. A knife edge from a utility knife is used to evaluate sharp features via the *modulation transfer function* (MTF). To analyse the image quality, a botanical sample (rosebuds) are used. The sample position can be freely adjusted depending on the desired magnification. Further, the samples are mounted on a rotation stage. Here we analyse the effects of different interpolation methods (nearest neighbour, linear, cubic, makima, and spline), super-resolution factors (interpolation factors), amount of low-resolution images, and the translation of the sample on the detector on the resulting high-resolution images.

2.2 Super-resolution

Super-resolution is achieved by registering the shift between individual images with sub-pixel precision [4], interpolating the images on a high-resolution grid [5], and averaging the interpolated images [1, 2, 5]. Using pixel detectors, this method is sufficient to obtain high quality images [2]. However, using a CCD or CMOS camera will require post-processing using a deconvolution filter, e.g. a Wiener filter [1], Richardson-Lucy filter, regularisation filter [6], or a blind deconvolution [6–8]. Considering conventional cameras, the blur kernel (PSF or a Gaussian) can also be extracted from the image resulting in a *blind* method [6, 7]. We remove pixel errors and apply flat-field correction before processing [2]. Sroubek et al. [6, 8] state that the theoretical resolution increase R is given by:

$$R = \lceil \sqrt{n_{\text{img}}} \rceil - 1. \tag{2.1}$$

Where $\lceil\rceil$ represents the ceil function and n_{img} the amount of low-resolution images.

There are several alternative methods to obtain super-resolution. Irani et al. proposed an iterative back-projection algorithm [9] and Sroubek et al. utilise a unified approach related to image regularisation [6]. The method to estimate super-resolution images can be tailored to the specific setup or sample. Greenspan et al. proposed a method based on *projection onto convex sets* (POCS) to be used in medical super-resolution imaging [10]. Viermetz et al. showed that super-resolution improves spatial resolution to a higher degree than increasing geometric magnification using a Talbot interferometer and a biological sample [11]. We employ a generalised approach that does not rely on detailed knowledge on the sample nor the setup, as described by Milanfar [1] adjusted for pixel detectors as described above [2].

The described approach can be applied to *computed tomography* (CT) as well [2]. For every projection, one super-resolution image is estimated. After preparing the projections, the sample can be reconstructed. In this paper, we use the *MuhRec* software set to cone beam geometry for 360° rotation, applying tilt correction, ring filtering, and cropping [12].

2020 JINST 15 C03002

2.3 Image quality analysis

To quantify the quality of sharp features in an image, the *slanted edge* method [13] is used, which utilises the MTF. For this method a sharp edge is tilted by a few degrees. From a region of interest, a column or row is chosen giving an *edge spread function* (ESF). From the ESF, a *spatial frequency response* (SFR) can be created, which is then derived to obtain the *line spread function* (LSF). Finally, the MTF is obtained via Fourier transformation of the LSF. The resulting MTF is truncated using the FWHM obtained by applying a Gaussian fit to the LSF [13–15].

The *signal to noise ratio* (SNR) and *contrast to noise ratio* (CNR) are methods to determine the quality of an image without requiring a reference image. The SNR is defined as:

$$SNR = 20 * \log \frac{s}{n_{\mathrm{RMS}}}. \tag{2.2}$$

Where s is the mean value of a region containing the sample and n_{RMS} is the *root mean square* (RMS) of a region without sample, which is defined as: $n_{\mathrm{RMS}} = \sqrt{{n_{\mathrm{mean}}}^2}$ where n_{mean} is the mean value of the region without sample.

The CNR is defined as:

$$\mathrm{CNR} = \frac{\mid s - n \mid}{\sigma_n}. \tag{2.3}$$

Where s is the mean value of a region containing the sample, n is mean value of a region without sample, and σ_n is the standard deviation of the region without sample [16]. The regions are equally sized and manually chosen. The same regions can be used for both SNR and CNR calculations.

For an additional quantitative comparison of the image quality, the radial power spectrum is used. Therefore, the images are Fourier transformed, radially integrated, and plotted in double logarithmic representation as function of the spatial frequency. The resulting power spectrum is truncated at the Nyquist frequency [17] and maximum and minimum spatial frequencies are obtained via equations (2.4).

$$f_{\mathrm{nyquist}} = \frac{{p_{\mathrm{size}}}^{-1}}{2}, \qquad f_{\mathrm{max}} = {p_{\mathrm{size}}}^{-1}, \qquad f_{\mathrm{min}} = \frac{(n_{\mathrm{pix}} * p_{\mathrm{size}})^{-1}}{2}. \tag{2.4}$$

Where p_{size} is the pixel size in mm and n_{pix} is the amount of pixels in x direction.

3 Results

3.1 Super-Resolution images

Compared to a single image, super-resolution has in all our tests improved the image regardless of the interpolation method, amount of images, translation of the sample on the detector, or interpolation factor. Good results have been achieved using 4×4 images with a sample translation of 3 pixels and 4 times spline interpolation (see figure 1(a)). In figure 1(b), it can be observed that cubic, makima, and spline interpolation appear sharper than linear or nearest neighbour interpolation.

3.2 Image quality

When comparing different interpolation methods, the MTF (figure 2(a)) shows that spline performs best on sharp features. Nearest neighbour interpolation performs better than expected in this case,

2020 JINST 15 C03002

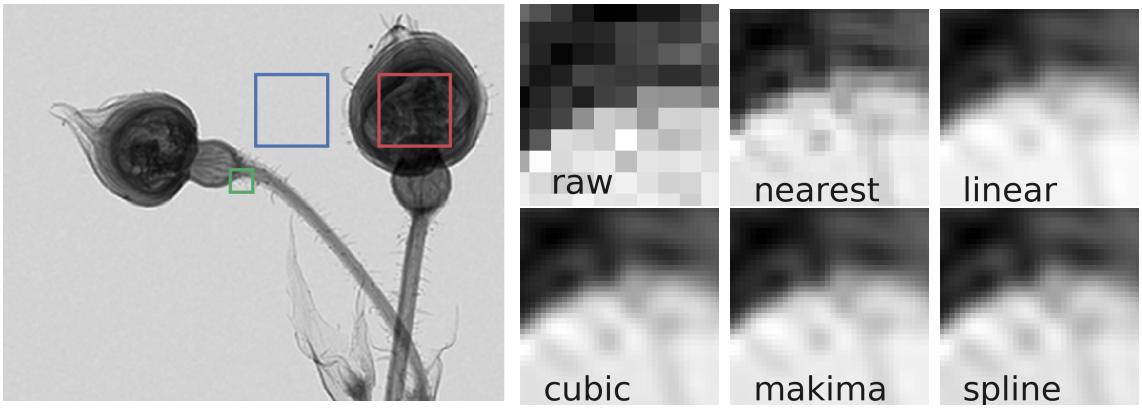

(a) (b)

Figure 1. (a) Super-resolution image (rosebuds) created from 4×4 images, 3 pixels sample translation, and 4 times spline interpolation. The red and blue squares have been used for SNR and CNR calculations. (b) Zoom of the green square shown in (a) with different interpolation methods as indicated.

while linear interpolation yields the poorest MTF. However, the observed differences are very small. Considering the SNR and CNR (figure 2(b)), it can be observed that cubic and makima interpolation provide a slightly higher CNR and the SNR is almost unaffected. The radial power spectrum (figure 2(c)) is very similar for all methods and degrades for higher spatial frequencies.

Using a varying amount of images with 4 times interpolation and 3 pixels sample translation shows that the effect on the MTF is small, but spline performs well for 4×4 and 5×5 images (figure 3(a)). Again, the SNR (figure 3(b)) is almost unaffected, while the CNR increases with the amount of images. Figure 3(c) shows that the power spectrum performs slightly better for super-resolution images compared to a single position (reference image). Increasing the interpolation factor considering 4×4 images with 3 pixels sample translation shows that the interpolation factor can be increased up to factor 5 before the MTF shows significant changes (figure 4(a). Figure 4(b) shows that SNR and CNR are almost unaffected. The radial power spectrum (figure 4(c)) degrades with increasing interpolation but performs slightly better than a single position (reference image).

Considering the total translation of the sample on the detector using 4×4 images, the MTF and power spectrum for 3 pixels perform well (figures 5(a) and 5(c)) Again, the SNR is almost unaffected and the CNR increases with the sample translation (figure 5(b)).

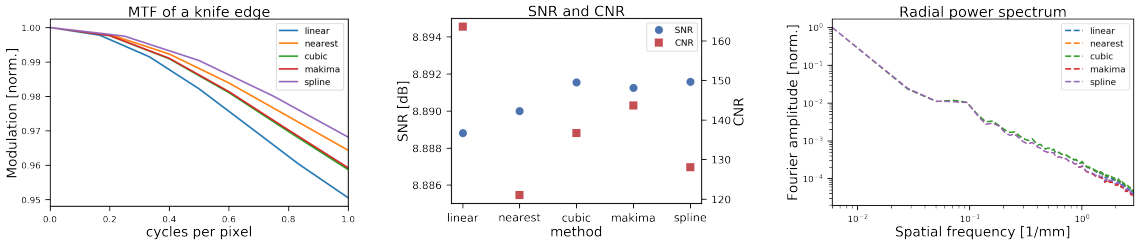

(a) (b) (c)

Figure 2. Different interpolation methods using 4×4 images, 3 pixels sample translation, and 4 times interpolation. (a) MTF. (b) SNR and CNR. (c) radial power spectrum.

2020 JINST 15 C03002

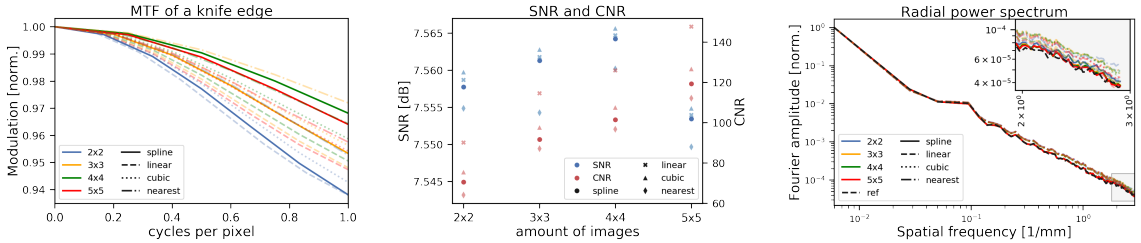

(a) (b) (c)

Figure 3. Varying the amount of low-resolution images using 3 pixels sample translation, and 4 times interpolation. (a) MTF. (b) SNR and CNR. (c) radial power spectrum.

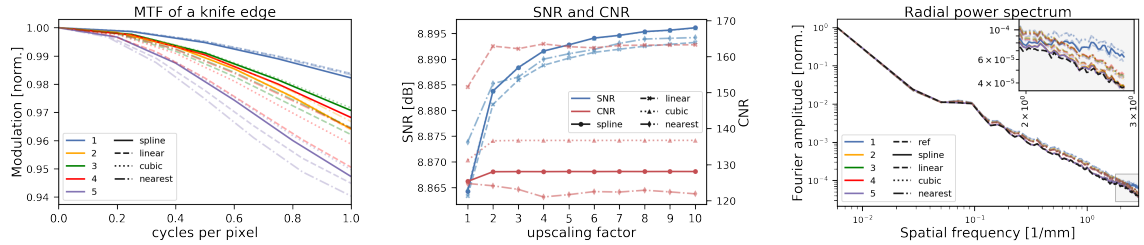

(a) (b) (c)

Figure 4. Varying the interpolation factor using 4×4 images, 3 pixels sample translation. (a) MTF. (b) SNR and CNR. (c) radial power spectrum.

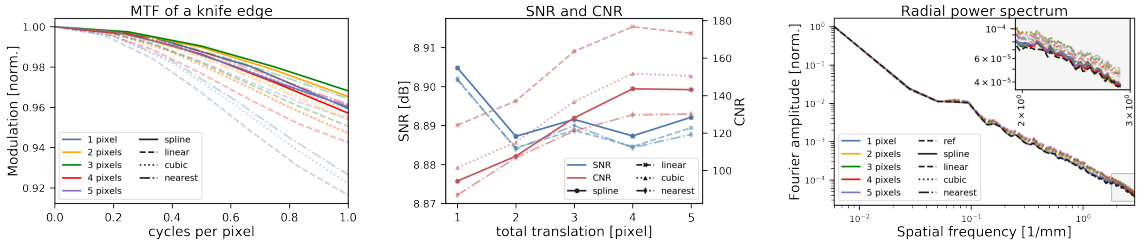

(a) (b) (c)

Figure 5. Varying the translation of the sample on the detector using 4×4 images and 4 times interpolation. (a) MTF. (b) SNR and CNR. (c) radial power spectrum.

3.3 Super-resolution tomography

This demonstration has been performed with 360 projections. To reduce the scan time, 2×2 images with a sample translation of 3 pixels and 2 times spline interpolation are used. In figure 6(a) a regular CT is shown and in figure 6(b) the super-resolution CT of the same sample is shown. Comparing both scans shows that more details can be observed in the super-resolution CT, e.g. thorns on the stems (figures 6(c) and 6(d)). Further, artefacts in the reconstruction are also reduced due to longer total exposure of each individual projection in the super-resolution CT.

2020 JINST 15 C03002

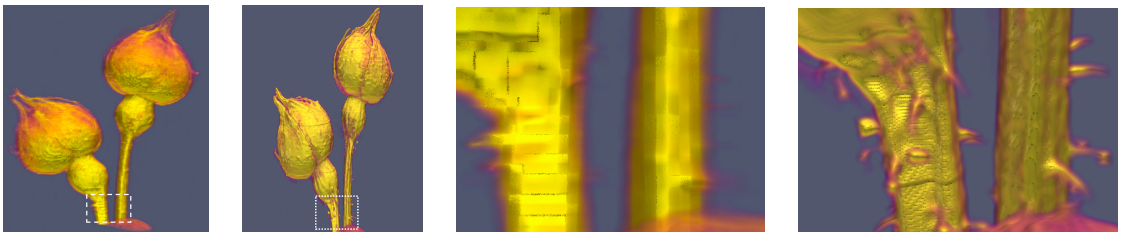

(a) (b) (c) (d)

Figure 6. Reconstruction of 2 rosebuds from 360 projections. (a) regular CT. (b) super-resolution CT using 2×2 images. (c-d) zoom of the highlighted areas in (a) and (b).

4 Discussion and conclusions

It has been demonstrated that hybrid pixel detectors are well suited for super-resolution imaging. The method can be applied to CT as well increasing the amount of detail in the reconstruction.

The most significant visual improvement of the estimated high-resolution images comes from the chosen interpolation method. Spline and cubic interpolation seem to be a good choice considering visual and measurable features. As expected, SNR is largely unaffected by the interpolation method or the amount of images. The MTF also shows only very minor changes. Also, the power spectrum only show very minor differences. The CNR, however, is a good measure to judge image quality in these experiments regardless of interpolation method.

Theoretically, it should be sufficient to translate the sample for a maximum of 1 pixel to obtain sufficient details. However, our experiments have shown that 3 pixels might be more suited considering 4×4 images. This case is less sensitive to tolerances of the X-ray spot positions, accounts for difference between individual pixels and the 3D structure of the sample. Shifts between individual images should always be a fraction of a pixel for maximum new information. Being able to precisely control the X-ray spot position is highly beneficial for such applications.

Acknowledgments

This project is financially supported by the Swedish Foundation for Strategic research (SSF) Grant No. ID17-0097.

References

[1] P. Milanfar, *Super-resolution imaging*, CRC Press, Boca Raton, U.S.A. (2010).

[2] K.R. Rix, T. Dreier, T. Shen and M. Bech, *Super-resolution X-ray phase-contrast and dark-field imaging with a single 2D grating and electromagnetic source stepping*, *Phys. Med. Biol.* **64** (2019) 165009-

[3] B. Henrich et al, *PILATUS: a single photon counting pixel detector for X-ray applications*, *Nucl. Instrum. Meth.* **A 1** (2009) 247.

[4] M. Guizar-Sicairos et al, *Efficient subpixel image registration algorithms*, *Opt. Lett.* **33** (2008) 156.

2020 JINST 15 C03002

[5] A. Gilman et al, *Interpolation models for image super-resolution*, *IEEE Int. Sym. Elect. Des.* (2008) 55.

[6] F. Sroubek, G. Cristobal and G.J. Flusser, *A unified approach to super-resolution and multichannel blind deconvolution*, *IEEE Trans. Image. Process.* **19** (2007) 2322.

[7] T. Michaeli and M. Irani, *Nonparametric blind super-resolution*, *IEEE Int. Conf. Comp. Vis.* (2013) 945.

[8] F. Sroubek and J. Flusser, *Multichannel blind deconvolution of spatially misaligned images*, *IEEE Trans. Image. Process.* **14** (2005) 874.

[9] M. Irani and S. Peleg, *Improving resolution by image registration*, *CVGIP-Graph. Model. Im.* **53** (1991) 231.

[10] H. Greenspan, *Super-resolution in medical imaging*, *Computer J.* **52** (2008) 43.

[11] M. Viermetz et al. *High resolution laboratory grating-based X-ray phase-contrast CT*, *Sci. Rep.* **8** (2018) 15884

[12] A.P. Kaestner, *MuhRec — A new tomography reconstructor*, *Nucl. Instrum. Meth.* **A 651** (2011) 156.

[13] M. Estribeau and P. Magnan, *Fast MTF measurement of CMOS imagers using ISO 12333 slanted-edge methodology*, *P. Soc. Photo-Opt. Ins.* **5251** (2004) 243.

[14] A.S. Chawla, H. Roehrig, J.J. Rodriguez and J. Fan, *Determining the MTF of medical imaging displays using edge techniques*, *J. Digit. Imag.* **18** (2005) 296.

[15] T. Dreier et al., *A USB 3.0 readout system for Timepix3 detectors with on-board processing capabilities*, 2018 *JINST* **13** C11017.

[16] A. Velroyen et al., *Microbubbles as a scattering contrast agent for grating-based X-ray dark-field imaging*, *Phys. Med. Biol.* **58** (2013) N37.

[17] M. Bech, et al., *X-ray imaging with the PILATUS 100k detector*, *Appl. Radiat. Isot.* **66** (2008) 474.

2020 JINST 15 C03002